REPORT DOCUMENTATION PAGE

Form Approved OMB No. 0704-0188

1. REPORT DATE *(DD-MM-YYYY)*	2. REPORT TYPE	3. DATES COVERED *(From - To)*
March 2001	Journal article	9/97 - 12/98

4. TITLE AND SUBTITLE
Characterizing Fluorine and Chlorine Atom Flow Rates Using Iodine Atom Spectrometry

5a. CONTRACT NUMBER

5b. GRANT NUMBER

5c. PROGRAM ELEMENT NUMBER

6. AUTHOR(S)
Gerald C. Manke II, Thomas L. Henshaw, Timothy J. Madden, John M. Herbelin, Brent D. Rafferty, Gordon D. Hager

5d. PROJECT NUMBER
3326

5e. TASK NUMBER
LA

5f. WORK UNIT NUMBER
02

7. PERFORMING ORGANIZATION NAME(S) AND ADDRESS(ES)

Air Force Research Laboratory
Directed Energy Directorate
3550 Aberdeen Ave. SE
Kirtland AFB, NM 87117

8. PERFORMING ORGANIZATION REPORT NUMBER

9. SPONSORING / MONITORING AGENCY NAME(S) AND ADDRESS(ES)
Air Force Research Laboratory
Directed Energy Directorate
3550 Aberdeen Ave. SE
Kirtland AFB, NM 87117

10. SPONSOR/MONITOR'S ACRONYM(S)

12. DISTRIBUTION / AVAILABILITY STATEMENT
Approved for public release; distribution is unlimited

13. SUPPLEMENTARY NOTES
AIAA Journal, Vol. 39, No. 3, March 2001, pp. 447 - 454

14. ABSTRACT
The production of F and Cl atoms in an electrical discharge of F2 or Cl2 has been examined in a flow reactor. A tunable diode laser was used to probe the concentration and translational temperature of I atoms produced by F and Cl atom reactions with HI. Kinetic modeling codes were used to determine the discharge efficiencies from the titration plots and the observed trends for atom concentration as a function of F2 or Cl2 and pressure. These calculations indicated that the DC discharge used in these experiments is 100% efficient for F2 flow rates <= 0.5 mmol/s and reactor pressure <= 20 Torr. The highest F2-free F atom flow rate that we can generate is 1.0 mmol/s. Preliminary data for the Cl2 discharge indiate that this is a much less efficient source of Cl atoms with yields of less than 50%.

15. SUBJECT TERMS
halogen atom titrations, tunable diode laser spectrometry, DC discharges, gas phase titrations, subsonic flow reactors

16. SECURITY CLASSIFICATION OF:			17. LIMITATION OF ABSTRACT	18. NUMBER OF PAGES	19a. NAME OF RESPONSIBLE PERSON
a. REPORT	b. ABSTRACT	c. THIS PAGE	Unlimited	10	Gerald C. Manke II
Unclassified	Unclassified	Unclassified			19b. TELEPHONE NUMBER *(include area code)* 505-853-2674

Characterizing Flourine and Chlorine Atom Flow Rates Using Iodine Atom Spectrometry

G. C. Manke II, T. L. Henshaw, T. J. Madden,
J. M. Herbelin, B. D. Rafferty, G. D. Hager

Reprinted from

AIAA Journal

Volume 39, Number 3, Pages 447–454

A publication of the
American Institute of Aeronautics and Astronautics, Inc.
1801 Alexander Bell Drive, Suite 500
Reston, VA 20191–4344

AIAA JOURNAL
Vol. 39, No. 3, March 2001

Characterizing Fluorine and Chlorine Atom Flow Rates Using Iodine Atom Spectrometry

Gerald C. Manke II,* Thomas L. Henshaw,† Timothy J. Madden,‡
John M. Herbelin,§ Brent D. Rafferty,† and Gordon D. Hager¶
U.S. Air Force Research Laboratory, Kirtland Air Force Base, New Mexico 87117-5776

The production of F and Cl atoms in an electrical discharge of F_2 or Cl_2 has been examined in a flow reactor. A tunable diode laser was used to probe the concentration and translational temperature of I atoms produced by F and Cl atom reactions with HI. Kinetic modeling codes were used to determine the discharge efficiencies from the titration plots and the observed trends for atom concentration as a function of F_2 or Cl_2 and pressure. These calculations indicate that the dc discharge used in these experiments is 100% efficient for F_2 flow rates $\leq$0.5 mmol s^{-1} and reactor pressure $\leq$20 torr. The highest F_2-free F atom flow rate that we can generate is 1.0 mmol s^{-1}. Preliminary data for the Cl_2 discharge indicate that this is a much less efficient source of Cl atoms with yields of less than 50%.

Introduction

SINCE their invention in the mid 1960s, the most widely studied class of chemical lasers has been the hydrogen halide systems.[1] These lasers operate on an exothermic energy release whereupon the liberated energy is deposited into newly formed hydrogen halide bonds to produce a population inversion between vibrational levels. The following three-atom exchange reactions typify the pumping reaction for producing upper vibrational levels in hydrogen halides:

$$X + H_2 \rightarrow HX(v) + H \tag{1}$$

$$X + HY \rightarrow HX(v) + Y \tag{2}$$

$$H + X_2 \rightarrow HX(v) + X \tag{3}$$

where X and Y are the halogens F, Cl, Br, I, and H can be replaced by deuterium D. In some cases, more than 50% of the available exothermicity is channeled into product vibration[2] and high vibrational levels, up to $v = 10$, can be populated. However, lasing usually occurs on $\Delta v = -1$ and -2 transitions between the low-lying vibrational levels. For example, the prominent rovibrational laser lines for the HF laser lie in the $(v'' = 2 \rightarrow v' = 1)$ and $(v'' = 1 \rightarrow v' = 0)$ bands between 2.5 and 3.0 μm.

Recently, a population inversion and lasing were reported by this laboratory on the atomic iodine $I(^2P_{3/2})$–$I(^2P_{1/2})$ transition at 1.315 μm using the following energy transfer process[3–7]:

$$NCl(a^1\Delta) + I\left(^2P_{\frac{3}{2}}\right) \rightarrow NCl(X^3\Sigma^-) + I^*\left(^2P_{\frac{1}{2}}\right) \tag{4}$$

This system is analogous to the well-known chemical oxygen iodine laser (COIL).[8] The $NCl(a^1\Delta)$ metastable ($T_0 = 1.1$ eV) is isovalent to singlet oxygen in COIL and undergoes an efficient energy transfer reaction similar to the $O_2(a^1\Delta) + I(^2P_{3/2})$ reaction in COIL. However, in this scheme the $NCl(a^1\Delta)$ is generated through a purely gas-phase chemical reaction mechanism

$$Cl + HN_3 \rightarrow HCl + N_3 \tag{5}$$

$$Cl + N_3 \rightarrow NCl(a^1\Delta) + N_2 \tag{6}$$

and, as such, represents a significant breakthrough in chemical laser technology.

It should be noted that reactions (1–6) are preceded by a complex set of chain chemistry where the free radicals X and/or H are generated in the initial steps. There are many methods for generation of these radicals, including electrical and microwave discharges, photolysis, and purely chemical means such as high-temperature combustors. The coupling of high-enthalpy flows found in chemical lasers with these radical generator schemes produces large amounts of heat in the active medium. Thus, extracting efficient continuous wave laser operation involves managing homogeneous reagent mixing times and thermal budgets of the active medium with respect to the kinetics of the system. Through optimization of several flowfield parameters such as gas temperature, velocity, and species density, an appropriate laser resonator and sub- or supersonic nozzle design can be fashioned to accommodate the extreme heat release and mixing requirements found in these systems. Because these parameters are variable, the laser output power/efficiency will fluctuate accordingly, and a systematic choice of operational conditions is required for efficient operation. This is especially true of the hydrogen halide lasers because the vibrational distribution and small signal gain can vary widely with operating conditions. The $NCl(a^1\Delta)/I^*(^2P_{1/2})$ laser system is also sensitive to operating conditions. For example, to optimize the $NCl(a^1\Delta)$ and $I^*(^2P_{1/2})$ generation, complete dissociation of F_2 or Cl_2 is essential because IF and ICl, which are generated by

$$I + X_2 \rightarrow IX + X \tag{7}$$

[where $k_F = 4.5 \times 10^{-14}$ and $k_{Cl} = 5.5 \times 10^{-14}$ cm^3 $molecule^1$ s^{-1} (Refs. 9 and 10)] rapidly quench $NCl(a^1\Delta)$ (Ref. 11) and $I^*(^2P_{1/2})$. Note that $k(I + Cl_2)$ is estimated to be the same as $k[I^*(^2P_{1/2}) + Cl_2]$ (Ref. 10).

Indeed, most chemical lasers and other high-temperature reacting flows contain complex chemical and fluid dynamical processes that require facile temporal and spatial resolution. Before the advent of tunable diode lasers, the data required to fully characterize these systems were difficult to obtain. However, a species' concentration and temperature can now be readily characterized through its spectral absorption features using commercial narrow-line tunable diode lasers. The resulting spatially resolved, high-fidelity, and high-resolution data are particularly useful for characterizing the complex environment found in chemical lasers.

In this paper, we expand on our earlier report of a versatile titration technique that measures F atom densities by using a laser-based absorption technique.[12] The data reduction methodology has been refined, and a one-dimensional computational fluid mechanics analysis has been applied. Although this methodology is a general

Received 16 December 1999; revision received 20 July 2000; accepted for publication 26 July 2000.

*National Research Council Postdoctoral Fellow, Directed Energy Directorate, High Power Gas Lasers Branch, 3550 Aberdeen Avenue SE.

†Research Chemist, Directed Energy Directorate, High Power Gas Lasers Branch, 3550 Aberdeen Avenue SE.

‡Aerospace Engineer, Directed Energy Directorate, High Power Gas Lasers Branch, 3550 Aberdeen Avenue SE.

§Senior National Research Council Fellow, Directed Energy Directorate, High Power Gas Lasers Branch, 3550 Aberdeen Avenue SE.

¶Technical Director, Directed Energy Directorate, High Power Gas Lasers Branch, 3550 Aberdeen Avenue SE.

technique for characterizing F or Cl atom concentrations produced from combustion or electrical discharge devices, our specific interest is to find conditions where large F_2 and Cl_2 free flows of F or Cl atoms could be generated using an electric discharge because molecular halogens and interhalogens are deleterious quenchers of $NCl(a^1\Delta)$ and $I^*(^2P_{1/2})$.

Experimental Methods

A. X + HI Atom Titration

In these experiments, F and Cl atoms are generated by a commercial electric (dc) discharge (Helios, Inc.) in F_2 or Cl_2. Optical absorption methods for determining absolute concentration of these atomic species is difficult because the lowest energy allowed transitions for F and Cl atoms lie in the vacuum UV.[13–15] The $^2P_{3/2}$–$^2P_{1/2}$ spin-orbit transitions[16] for F and Cl, 404 and 881 cm^{-1}, respectively, can be probed directly,[17,18] but the signals are quite weak and a commercial source for a 404-cm^{-1} laser no longer exists. To circumvent these problems, titration methods have been developed, where a chemical reagent that reacts with X is added to the flow to produce a species that can be readily detected and converted into absolute concentration. For example, a sensitive technique for detecting F atoms in a flow tube involves monitoring the intensity of HF ($v''=3\rightarrow v''=0$) chemiluminescence at 880 nm generated by $F + C_2H_6$ reactions while adding CF_3I as an F atom titrant.[19] This method is well suited for small flows of F, but would be quite expensive and difficult to implement in our large flow reactor. The most common methods for detecting the presence of Cl in a flow are resonance fluorescence and Cl_2 afterglow. Unfortunately, the titrants ClNO and C_2H_3Br are not appropriate or cost effective for our conditions (high flow rates and high pressure). In addition, these methods do not allow for simultaneous concentration and temperature measurement, as well as two-dimensional spatial resolution of the F and Cl density in the flow.

Unlike most techniques that involve the removal of a halogen-dependent chemiluminescent signal as a function of added titrant concentration, we monitor the generation of I atoms from the reaction between a halogen atom (X = F or Cl) and hydrogen iodide using an 1.315-μm diode laser to probe the $I(^2P_{3/2}) - I(^2P_{1/2})$ spin-orbit transition:

$$X + HI \rightarrow HX + I \tag{8}$$

[where $k_F = 4.1\times10^{-11}$ and $k_{Cl} = 1.6\times10^{-10}$ cm^3 $molecule^{-1}$ s^{-1} (Ref. 20)]. The I atom absorption increases linearly with HI concentration [HI], until all of the X atoms have been consumed. On continued addition of HI, the I atom absorption reaches a maximum and levels off to a constant value. Ideally, there are no X or I atom loss processes, and the initial X concentration $[X]_0$ is given by the maximum [I] observed. Typically, however, at least one or more X or I atom loss processes are present, and $[X]_0$ is determined by analysis of the I vs HI plots measured at a variety of experimental conditions. In our case, one-dimensional fluid mechanics calculations were used to determine $[X]_0$ and the F and Cl atom production efficiency of our dc discharge.

B. Flow Reactor

A schematic of the stainless-steel flow reactor hardware is shown in Fig. 1a. The reactor is pumped by two Kinney 850 pumps in parallel, each equipped with a Roots blower. The main reactor channel is 5.08 cm wide by 1.91 cm high by 30.5 cm long in the flow direction. A 2.4-cm-diam dc discharge tube is mounted at its entrance. A constant current of 286 mA (~10 kV) is applied to generate a flow of F or Cl atoms when a 20% F_2/He mixture or Cl_2 diluted with He are passed through the tube. The bulk He diluent is added at the interface between the main reactor and the end of the discharge tube. Hydrogen iodide (99%, Matheson) diluted in He is usually added to the flow stream through injectors located along the top and bottom of the reactor. These injectors consist of one row of 21 0.081-cm-diam holes and one row of 42 0.041-cm-diam holes. The first pair is located 7.0 cm downstream of the discharge exit, whereas the second pair of identical injectors (not used in this experiment) is located 1.8 cm farther downstream and is purged by a small flow of He. An axial ring injector located at the exit of the discharge tube is also available for injection of reagents. The location of pressure transducers and thermocouples is also indicated in Fig. 1a.

The output of the diode laser probe passes through Borofloat windows (with a 3-deg wedge to prevent etalon effects) attached to both sides of the main reactor channel. A $4.25\times1.91\times3.05$ cm^3 volume lies between the main reactor channel and both inner window surfaces. To prevent the expansion of the main reaction flow into these areas, stainless-steel containment shrouds were installed. A variety of shrouds were available depending on the reaction time of interest. In addition, purge flows of He were added at the windows and along the shrouds to balance the main He flow. These shrouds and purge flows not only define the effective path length for the probe laser (5 cm per pass), but also protect the windows from the corrosive chemical environment of the main flow.

The overall reactor pressure and linear flow velocity are controlled by adding a large flow of N_2 at the end of the reactor. The linear flow velocity is calculated using

$$V = \dot{M}RT/PA \tag{9}$$

where $\dot{M}$ is the total molar flow rate (typically ~130 mmol s^{-1}), A is the cross-sectional area (9.7 cm^2), R is the gas constant, P is the reactor pressure (10–30 torr), and T is the reactor temperature, determined from the I atom probe, vide infra. All reagent and diluent flows were controlled by calibrated MKS flow controllers or by the use of calibrated sonic orifices. The upstream temperatures are monitored by type T thermocouples (Omega) and the upstream pressures are controlled by a variety of manual and electronic pressure regulators (Proportion Air).

C. Diode Probe Laser

The optical path of the diode probe is shown schematically in Fig. 1b. The output from a tunable 1.3145-μm diode laser (New Focus Lasers Model 6248; bandwidth <500 kHz) is optically separated from the rest of the system by a Faraday isolator. Beamsplitters direct portions of the output into a Fabry–Perot etalon (Tec Optics SA-300) and a heated iodine (I_2) cell. The I_2 cell temperature is maintained at 650°C to produce a known concentration of I atoms that are used to confirm the proper operation of the laser. The main portion of the laser output is passed through a half-wave plate and a polarizing beam-splitting cube. The horizontally polarized component becomes the signal beam and is passed on to the reactor, while the vertically polarized component is reflected at 90 deg and is used as the reference. The angle of the half-wave plate is rotated to balance the signal and reference beam intensities. A pair of InGaAs detectors (Physical Sciences, Inc.) monitors the reference and signal intensities. Before transmission through the reactor, the linearly polarized signal beam is passed through a quarter-wave plate to convert it to circular polarization, and a telescope focuses the beam diameter to a 1-mm spot. A flat mirror located on the opposite side of the reactor reflects the signal beam back on itself. The return beam is separated at the quarter-wave plate and focused on the InGaAs detector. The signal beam can be translated along the length of the flow reactor to observe the temporal evolution of [I] and along the perpendicular axis to probe the vertical profile of the flow. The diode laser is computer controlled for rapid scans across the F = 3 – F = 4 hyperfine component of the I atom ($5p^5\ ^2P_{1/2}$–$^2P_{3/2}$) spin-orbit magnetic dipole transition. Acceptable signal to noise levels are achieved by 30–50 scans, and I atom number densities as low as $3-5\times10^{13}$ cm^{-3} can be routinely detected. Multiple passes through the reactor can easily lower this limit: Densities as low as 1×10^9 cm^{-3} can be detected with a 2-m path length (private communication, S. J. Davis, Physical Sciences, Inc., Andover, Massachusetts, 1998).

The iodine atom number density is derived from Beer's law:

$$I = I_0 e^{\gamma(\nu)L} \tag{10}$$

The path length L (two passes) is 10 cm, and $\gamma(\nu)$ is given by

$$\gamma(\nu) = \left(\tfrac{7}{12}\right)\left(\lambda^2 A_{3,4}/8\pi\right) f(\nu)\left[[I^*] - \tfrac{1}{2}[I]\right] \tag{11}$$

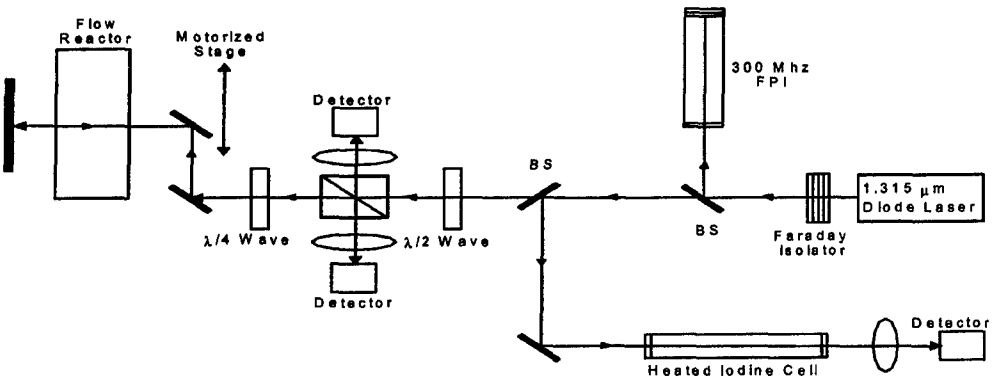

Fig. 1a Schematic diagram of the flow reactor; side view of the flow reactor shows the injection points for He (~130 mmol s^{-1}), F_2/Cl_2 (0.5–1.5 mmol s^{-1}), N_2, and HI (0.0–6.0 mmol s^{-1}).

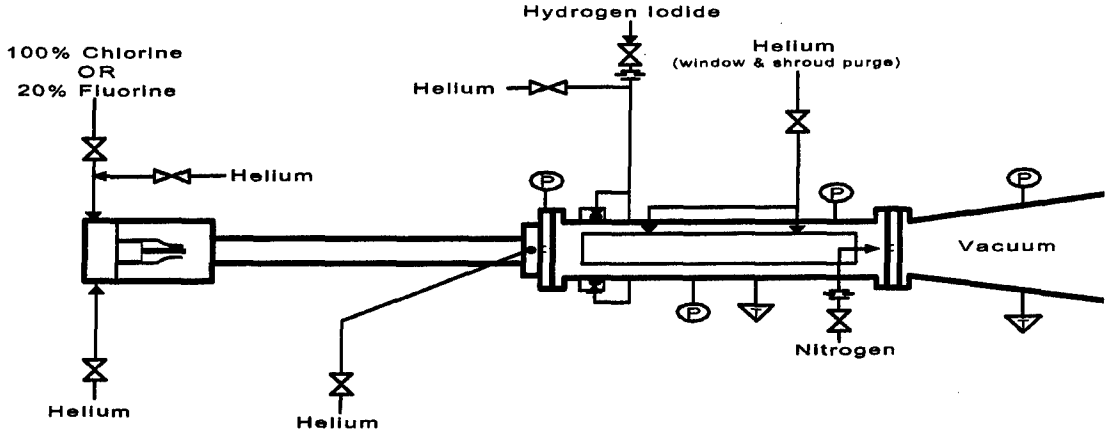

Fig. 1b Optical path for the I atom laser probe.

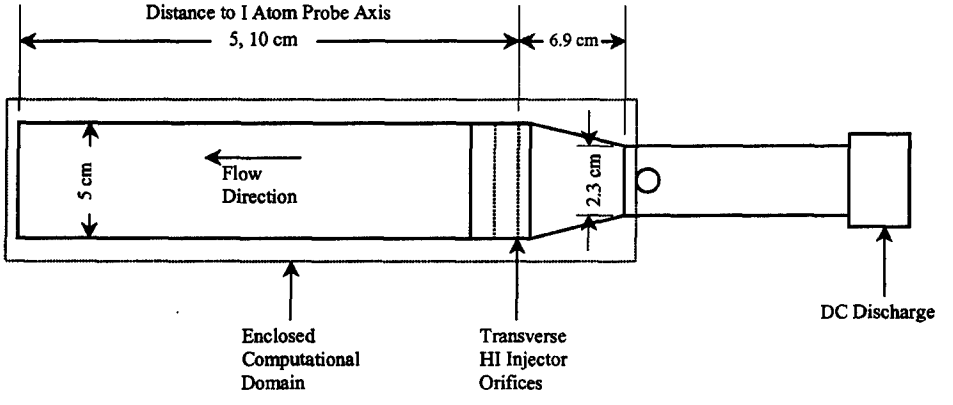

Fig. 1c Flow tube hardware and the computational domain used in the one-dimensional model; see text.

where A_{34} is the Einstein coefficient for the 3,4 hyperfine transition (5.08 s^{-1}), λ is wavelength (1.3145 μm), and $f(\nu)$ is the line shape function. For our conditions, $[I^*] = 0$, the inversion number density reduces to $\frac{7}{24}[I]$, and the ground-state density is obtained by integrating the gain over frequency:

$$\text{spectral area} \equiv \int_0^\infty \gamma(\nu)\,d\nu = -\frac{7}{24}\frac{\lambda^2 A_{3,4}}{8\pi}[I] \qquad (12)$$

The I atom spectra are fit by a Voigt function:

$$y = \text{spectral area} \times \frac{2\sqrt{\ln(2)}}{\pi^{\frac{3}{2}}} \times \frac{w_L}{w_G^2} \times \int_{-\infty}^{\infty} \left\{ e^{-t^2} \Big/ \left[\left(\sqrt{\ln(2)}\frac{w_L}{w_G} \right)^2 + \left(\sqrt{4\ln(2)}\frac{x - x_c}{w_G} - t \right)^2 \right] \right\} dt \qquad (13)$$

where w_G and w_L are the Gaussian and Lorentzian linewidths (full width at half maximum), respectively. If collisions with He are assumed to be the main source of broadening, the I atom translational temperature is calculated by

$$\text{temperature}\,(K) = M\left(w_G / 7.16 \times 10^{-7} \tilde{\nu}_0\right)^2 = 295/w_L \times 3.1 \times P_{He} \qquad (14)$$

where ν_0 is the line center of the transition (7607.5 cm^{-1}) and M is the atomic weight (126.9 g mol^{-1}). Example spectra and fits are shown in Fig. 2.

Based on the overall signal-to-noise ratio and the scatter of repeated temperature measurements at the same conditions, the relative error of the temperature measurement is assigned as ±30 K. The I atom density is given directly by the spectral area, and the error is quite small (<5%).

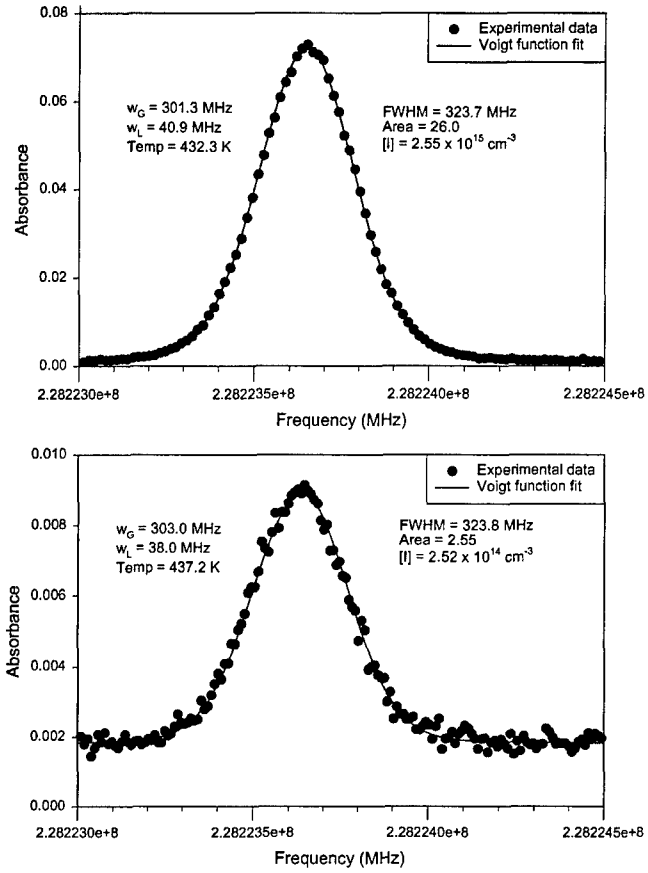

Fig. 2 Sample I atom spectra showing F = 3 − F = 4 hyperfine component of the I atom ($5p^5\ ^2P_{1/2}$–$^2P_{3/2}$) spin orbit magnetic dipole transition; signal-to-noise ratio is excellent and both spectra are well fit by a Voigt function.

The I atom flow rate is calculated by

$$\dot{I} = [I]^* V^* A \tag{15}$$

where V is given by Eq. (9) and A is the cross-sectional reactor area. Note that Eq. (15) can only be used if [I] is uniform along the vertical axis of the reactor. Because the velocity depends on both the temperature (±30 K) and total molar flow rate, we estimate that the I atom flow rate is reliable to within 15%. This is consistent with the systematic uncertainty normally associated with flow tube measurements.[21]

D. Fluid Mechanics Simulations: Methods

The model used in this investigation to analyze the experiment data is based on the generalized one-dimensional flow development of Shapiro.[22] This model describes the flow through a channel with changes in area and chemical composition, secondary mass injection, wall friction, and heat exchange with the duct walls. The flow changes are assumed to be continuous, and the gas is assumed to be real, with temperature-dependent specific heats. All chemical reactions are modeled with Arrhenius-type rate expressions for the forward rate. The equilibrium constant for each reaction is determined via the Gibb's free energy method (see Ref. 23), and the backward rate is calculated from the forward rate and the equilibrium constant.

The primary aspects of the model center on its ability to predict the changes in F atom number densities by three-body recombination, wall recombination, and reactions of F and F_2 with I and I_2. Hence, these aspects of the model are described in detail. The finite-rate chemistry and reactions used by our model are shown in Table 1 (see Refs. 24–31). The primary reactions are the production of I atoms via the reaction F + HI, the interhalogen reactions $F + I_2$ and $I + F_2$, and the atom recombination reactions. The vibrational distribution within HF produced by the F + HI reaction, the vibrational energy transfer reactions of HF, the energy transfer from HF(v) to I, and the deactivation of I* and HF(v) are listed for completeness, but affect the temperature and [I] predictions by only 5%. The primary reaction $F + HI \rightarrow HF + I$ has a nearly gas kinetic rate constant, as does the competing $F + I_2 \rightarrow IF + I$ reaction. Proper accounting for atom recombination, particularly in the case of I, is very important. The I atom recombination mechanism used here is based on the recommendations of Baulch et al.[9] for $M = He$, I_2, and arbitrary third-body partners. The Arrhenius rate constant expression for three-body recombination where $M = I$ was extrapolated from the data in Ref. 9 for both $M = I$ and I_2. The rate expression for $M = HI$ was determined by Chang and Burns[32] for the temperature range 200–323 K and is assumed to hold for the temperature range of concern here (400–600 K). For F atom recombination, we have adopted the recommendations of the 1977 U.S. Air Force Weapons Laboratory HF/DF kinetics review.[33]

Table 1 F + HI reaction rate constants

Reaction	k, cm^3 $molecule^{-1}$ s^{-1}	Reference
I atom production		
$F + HI \rightarrow HF(0) + I$	1.59×10^{-11}	9
$F + HI \rightarrow HF(1) + I$	1.91×10^{-11}	——
$F + HI \rightarrow HF(2) + I$	2.39×10^{-11}	——
$F + HI \rightarrow HF(3) + I$	2.55×10^{-11}	——
$F + HI \rightarrow HF(4) + I$	3.03×10^{-11}	——
$F + HI \rightarrow HF(5) + I$	3.98×10^{-11}	——
$F + HI \rightarrow HF(6) + I$	2.55×10^{-11}	——
Total	1.8×10^{-10}	——
Interhalogen reactions		
$F + I_2 \rightarrow IF + I$	4.3×10^{-10}	9
$I + F_2 \rightarrow IF + F$	1.9×10^{-14}	24
Three-body recombination		
$F + F + F \rightarrow F_2 + F$	$1.9 \times 10^{-8}\, T^{-1} \exp(629/T)$	
$F + F + F_2 \rightarrow F_2 + F_2$	$1.9 \times 10^{-8}\, T^{-1} \exp(629/T)$	
$F + F + M \rightarrow F_2 + M$	$7.8 \times 10^{-9} \exp(629/T)$	
$I + I + I \rightarrow I_2 + I$	$5.0 \times 10^{-33} \exp(2120/T)$	9
$I + I + HI \rightarrow I_2 + HI$	$3.8 \times 10^{-23} T^{-3.5}$	9
$I + I + I_2 \rightarrow I_2 + I$	$3.5 \times 10^{-33} \exp(2120/T)$	9
$I + I + M \rightarrow I_2 + M$	$5.5 \times 10^{-34} \exp(575/T)$	9
Wall recombination reactions		
$F + F + wall \rightarrow F_2 + wall$	$\gamma_F = 0.05$	25
$I + I + wall \rightarrow I_2 + wall$	$\gamma_I = 1.0$	26, 27
Energy transfer reactions		
$I^* + HF(0) \rightarrow I + HF(2)$	1.1×10^{-12}	28
$I^* + HF(0) \rightarrow I + HF(1)$	1.5×10^{-13}	——
$I^* + HF(0) \rightarrow I + HF(0)$	1.8×10^{-12}	——
$I^* + F_2 \rightarrow I + F_2$	5.0×10^{-14}	29
$I^* + I_2 \rightarrow I + I_2$	3.6×10^{-11}	30
$I^* + IF \rightarrow I + IF$	1.3×10^{-11}	31
$HF(v) + HF \rightarrow HF(v-1) + HF$, $v = 1$–6	$v(5.0 \times 10^{-10}\, T^{-1} + 5.8 \times 10^{-20}\, T^{2.26})$	1
$HF(v) + He \rightarrow HF(v-1) + He$, $v = 1$–6	$v(2.6 \times 10^{-30}\, T^5)$	——
$HF(v) + F_2 \rightarrow HF(v-1) + F_2$, $v = 1$–6	$v(1.3 \times 10^{-30}\, T^5)$	——
$HF(v) + F \rightarrow HF(v-1) + F$, $v = 1$–6	$v[2.7 \times 10^{-11} \exp(-1360/T)]$	——
$HF(v) + HF(v') \rightarrow HF(v+1) + HF(v'-1)$, $v = 1$–6, $v' \geq v + 2$, $v'(v+1) \leq 40$	$v'(v+1) 2.7 \times 10^{-11}\, T^{-1}$	——

Recombination of atoms at the channel walls is modeled via a source term in the species continuity equation of the form

$$\dot{J}_A = \gamma_A \sqrt{R_u T_w / 2\pi M_A} \left[\rho_{A_W} - \rho_{A_2,W} \left(\rho_A / \rho_{A_2} \right)_{eq} \right] \tag{16}$$

where γ_A is the recombination efficiency of species A, the subscript W pertains to properties in the gas at the wall, and the subscript eq indicates equilibrium conditions in the main body of the flow. The value of γ_F used here is 0.05, the maximum value determined by Kota et al.[25] at room temperature for all surfaces investigated including stainless steel. Note that the maximum value of γ_F reported by Kota et al. for any surface was 0.10 at 80 K, which indicates

that surface catalysis of F atom recombination is a relatively inefficient process. Kota et al. also report temperature dependent relations for Cl and Br atoms. (see Ref. 27). The I atom recombination coefficient used in this model is 1.0, based on the recommendations of Perram and Hager[26] and the work of Fisk and Hays.[27] This value is also consistent with the recombination coefficients recently reported by Kota et al. for Cl and Br atoms[34] (also see Ref. 26).

The computational domain for the physical space within the experiment simulated with this model extends from the exit of the discharge tube to the point at which the I atom measurements are taken in the streamwise direction, from wall to wall and shroud to shroud in the lateral direction, and from wall to wall in the vertical direction, see Fig. 1c. The discharge tube is treated as a black box entity, for which only the exiting mass flow is known; the pressure, temperature, and the F_2 dissociation fraction of the flow exiting the discharge tube are unknown quantities that are determined by matching the model predictions to measured quantities downstream. For the range of pressures, temperatures, and mass flow rates considered here, the flow exiting the discharge tube is subsonic, and in all simulations of the experiment, the flow is treated as subsonic throughout.

An important simplifying assumption of our calculations is that the HI/He flow is modeled with instantaneous mixing at the same streamwise position relative to the discharge tube exit at which the actual flow is injected. Secondary He is injected at the position of the second row of injectors, consistent with the experiment. Because the pressure across the injector orifices is always greater than 2:1, the sonic conditions are used to specify the temperature and pressure for each injectant flow.

The numerical technique used to solve the governing equations of the model is a first-order Adams–Bashfourth–Moulton method (see Ref. 35). In this numerical integration, the nominal step size Δx is 0.05 cm. This value was chosen by iteration until changes in the integrated solution were <1%. The step size after gas injection locations was decreased to $\Delta x/200$ and returned to Δx over a distance of $4\Delta x$. The solution is marched through the channel in the flow direction giving only upstream dependence and not directly capturing the elliptic nature of the subsonic flow. The calculated downstream pressure is determined by varying the inflow pressure until the model prediction and measurement agree. This technique is also used to match the experimentally determined temperatures. Reactant flow rates are input to the model as fixed quantities and are not affected by the pressure/temperature iterations.

Each titration represents a series of experiments where all parameters and flow rates are held constant except [HI]. As the HI flow rate approaches 0, the heat release of the F + HI reaction is minimized, and the flow conditions approach those for the flow without HI. Hence, the initial temperature exiting the discharge is determined by matching the temperature and pressure with the model for the lowest HI flow rate in the titration. On the other hand, because the F_2 dissociation fraction exiting the discharge tube is also unknown, this quantity is determined by matching the I atom number density measured for the highest HI flow in each titration series. The high [HI] data are used because they have the highest signal-to-noise ratio and are the least kinetic model dependent. With the dissociation fraction, pressure, and temperature fixed, the model is run for the remaining HI flow rates in the titration.

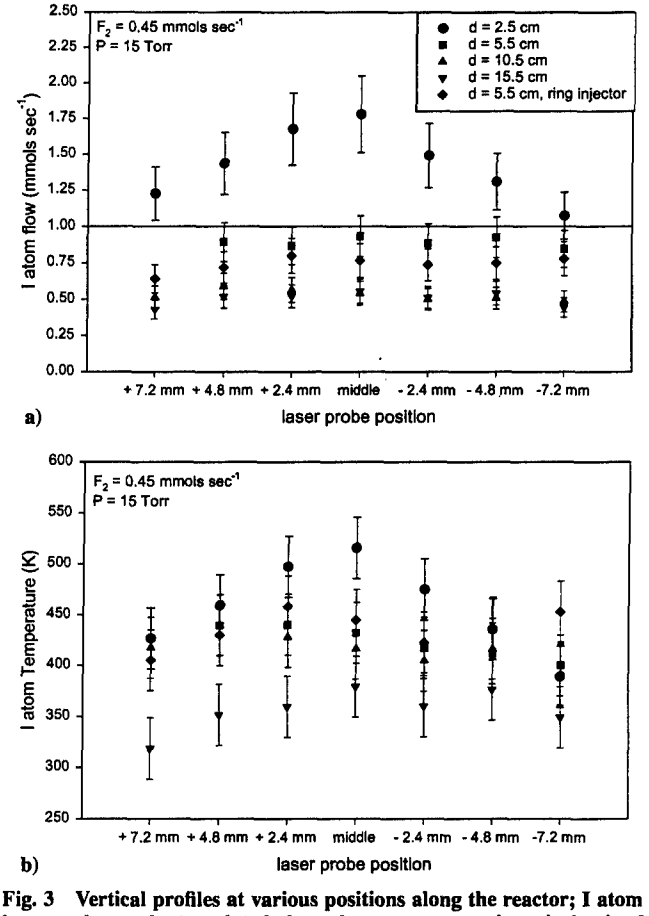

Fig. 3 Vertical profiles at various positions along the reactor; I atom laser probe can be translated along the transverse and vertical axis of the reactor. Profiles are flat for $d \geq 5.5$ cm.

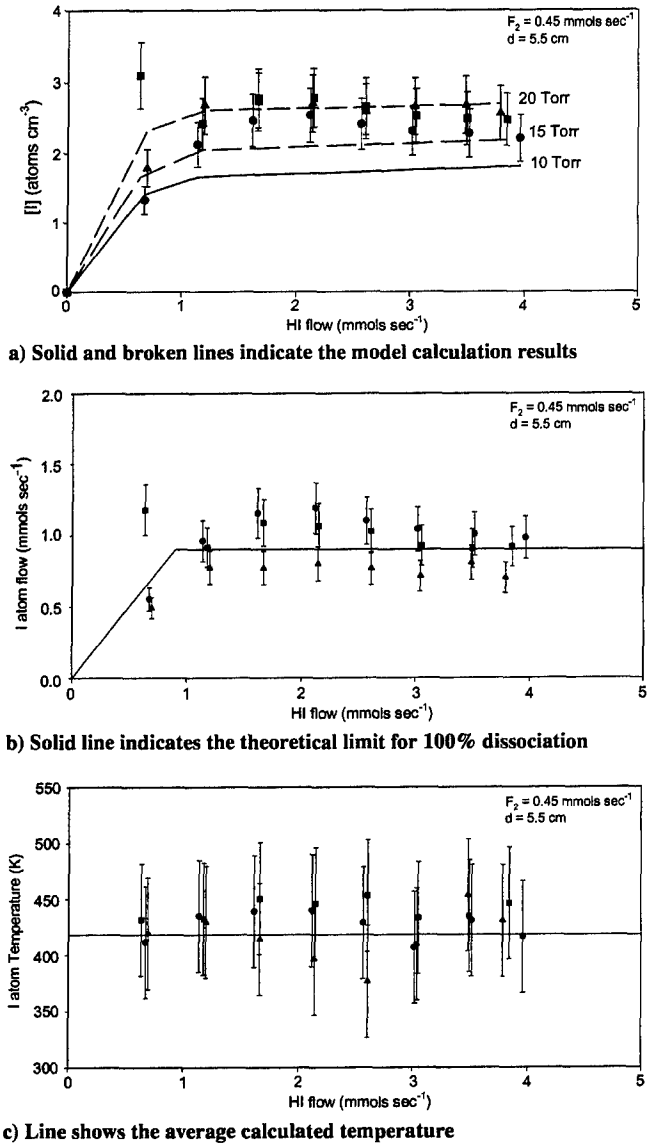

Fig. 4 Typical F + HI titration plots, I atom densities, I atom flow rates, and temperatures as a function of added HI at $F_2 = 0.45$ mmol s^{-1}: ●, $P = 12$ torr; ■, $P = 15$ torr; and ▲, $P = 20$ torr.

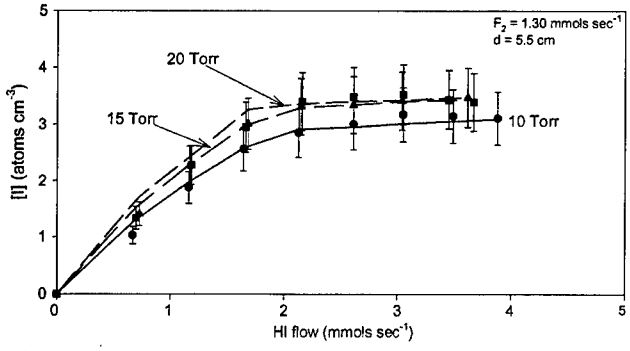

a) Solid and broken lines indicate the model calculation results

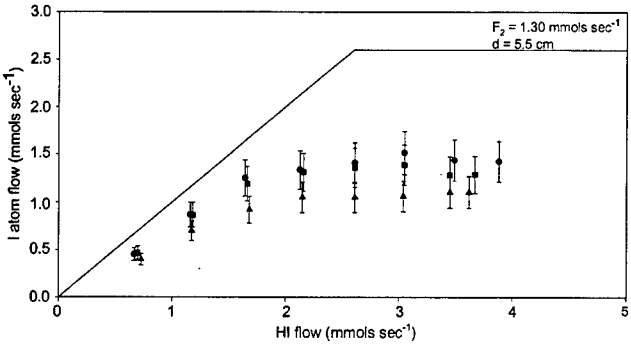

b) Solid line indicates the theoretical limit for 100% dissociation

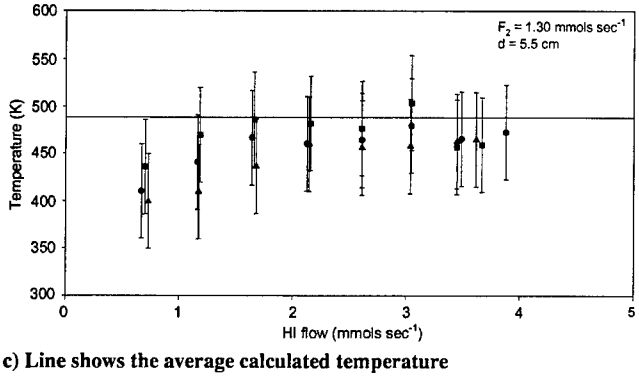

c) Line shows the average calculated temperature

Fig. 5 Typical F + HI titration plots, I atom densities, I atom flow rates, and temperatures as a function of added HI at $F_2 = 1.30$ mmol s^{-1}: ●, $P = 12$ torr; ■, $P = 15$ torr; and ▲, $P = 20$ torr.

Experimental Results

A. Vertical Profiles

An important advantage of our experimental technique is the ability to measure I atom concentrations and temperatures along both the transverse and streamwise directions of the flow reactor. Figure 3a shows the vertical profiles of the I atom flow rate measured at $F_2 = 0.45$ mmol s^{-1} with excess HI, $P = 15$ torr, and five different positions along the reactor. A uniform concentration profile should be exhibited, indicative of a constant velocity distribution along the vertical axis. The data measured 2.5 cm from the HI inlet are peaked in the center and fall off toward the edges. Clearly, a uniform flowfield has not been established and these data are not useful for determining [I] and T. The presence of at least one I atom loss process seems evident by the factor of 2 loss of I atoms between $d = 5.5$ and 15.5 cm. However, subsequent chemiluminescent measurements indicated significant flaring of the flow and leakage around the 10.5- and 15.5-cm flow containment shrouds. Consequently, only the 5.5 cm datum is considered to be reliable. Future reactor designs will resolve this problem. Figure 3b shows the I atom temperature profiles. At $d = 2.5$ cm, the temperature peaks in the center and is ~100 K lower at the edges. The I atom flow data violate mass balance, which indicates that the plug flow has not been established. As the distance between the reagent inlet and the observation point increases, the temperature decreases and the temperature profiles are no longer peaked.

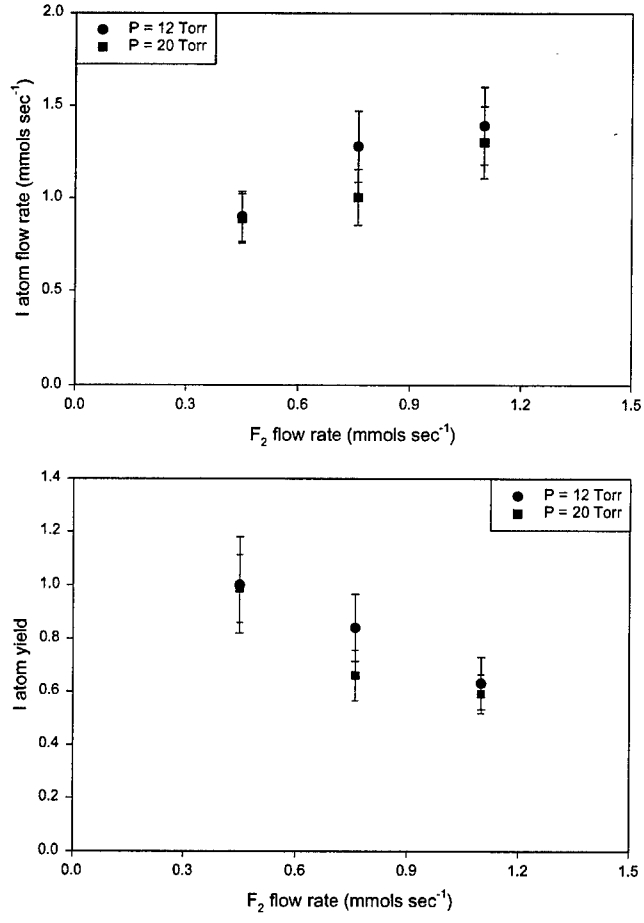

Fig. 6 I atom flow rate and I atom yield as a function of F_2.

B. F + HI Titrations

The data from six typical titrations are shown in Figs. 4 (0.45 mmol s^{-1} F_2) and 5 (1.3 mmol s^{-1} F_2). Figures 4a and 5a show [I] plotted vs the flow rate of added HI at three different pressures and $d = 5.5$ cm. In all cases, the titration plots have both a linear and a plateau region. Solid and broken lines indicate the model calculation results for [I]. Figures 4b and 5b show the corresponding I atom flow rates as a function of added HI, relative to the theoretical limit (indicated by the solid line), which assumes 100% dissociation of F_2, 1:1 stoichiometry, and no F or I atom losses. Finally, the measured temperatures are plotted Figs. 4c and 5c and are compared to the average values from the model calculations.

In all but one case, the model accurately reproduces the experimentally measured [I]; the only exception is for $P = 12$ torr and $F_2 = 0.45$ mmol s^{-1}, where the model underestimates [I]. However, as Fig. 4b shows, the I atom flow rate at 12 torr also exceeds the theoretical limit. Although this may be indicative of the flowfield problem described earlier, the error is only ~20%, and the problem is not serious. In general, however, the agreement between the model and the experiment is very good, with the values and slopes of the titration curves matched very well in most cases. The agreement between the model and experiment for the lower HI flow rates of each titration suggests that the mechanisms that interfere with a pure titration of F atoms (i.e., $I + F_2$, $F + I_2$, three-body recombination, and wall recombination) are modeled accurately. The average calculated temperature at 5.5 cm and $F_2 = 0.45$ mmol s^{-1} is 418 K, consistent with the experimental results. The data for $F_2 = 0.45$ mmol s^{-1} are also consistent with 100% dissociation. The dissociation efficiency is less than 70% for the data with $F_2 = 1.30$ mmol s^{-1} (see Fig. 5). The calculated temperature for $F_2 = 1.3$ mmol s^{-1} is higher than for $F_2 = 0.45$ mmol s^{-1}, $T_{av,calc} = 488$ K, and is consistent with the measured values. The agreement between the predicted temperatures via the line shape analysis and the model predictions tends to validate both the line shape analysis and the model.

Figures 6 and 7 summarize the titration results as a function of F_2 flow rate and pressure. In all three panels, the data points represent

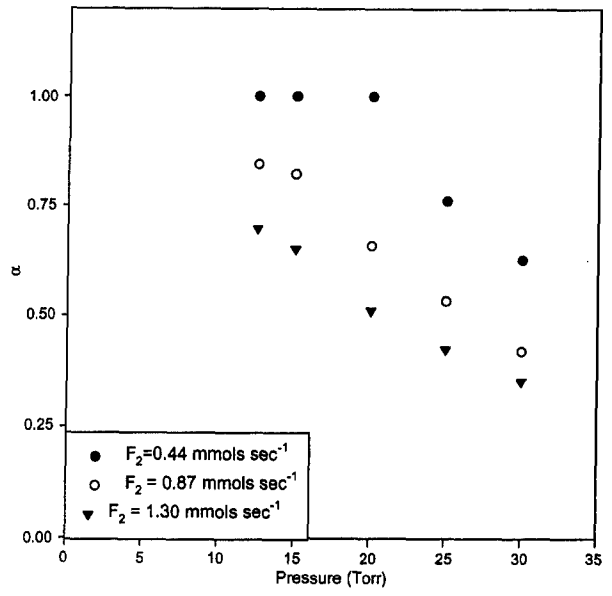

Fig. 7 Dissociation fraction vs pressure; F_2 dissociation fraction, $\alpha = I_{max}/2^*F_2$, is plotted as a function of the reactor pressure.

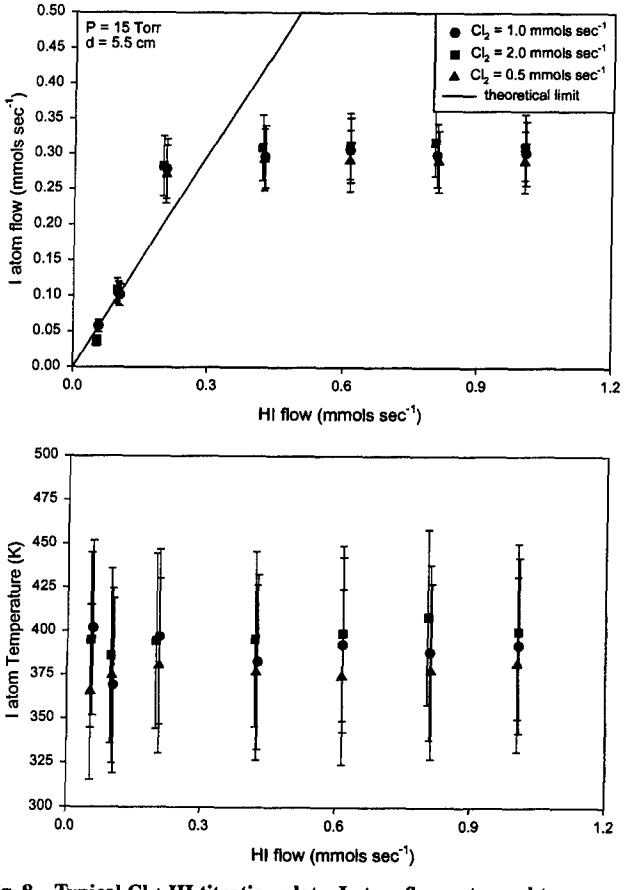

Fig. 8 Typical Cl + HI titration plots; I atom flow rates and temperatures as a function of added HI at a variety of experimental conditions.

the average I atom flow rate from the plateau region of the corresponding titration curves. Figure 6 demonstrates the effect of increased F_2, and although the I atom flow rate is shown to increase with larger F_2 flow rates, the I atom yield given by

$$\alpha \equiv \text{I atom yield} = \frac{\text{I atom flow rate}}{2^*\text{F}_2 \text{ flow rate}} \qquad (17)$$

is inversely proportional to the F_2 flow rate. These data indicate that both the F_2 flow rate and reactor pressure affect the performance of the dc discharge. The highest F_2-free flow rate of F atoms that we are capable of generating is 1.0 mmol s^{-1}. As shown in Fig. 7, for $F_2 \leq 0.44$ mmol s^{-1} and $P \leq 20$ torr, 100% dissociation is achieved. At higher F_2 flow rates and pressures, the dissociation efficiency decreases linearly.

C. Cl + HI Titrations

A set of typical Cl + HI titrations are shown in Fig. 8. The atom flow rate generated by the Cl_2 discharge is significantly smaller than that obtained from F_2. In addition, the temperature is slightly lower, $T \sim 400$ K. Increasing the Cl_2 flow rate does not generate more Cl atoms and increasing the pressure also degrades the discharge performance. The highest Cl atom flow rate that we can generate is 0.3 mmol s^{-1} independent of the initial flow rate of Cl_2, and the average temperature is ~380 K. The best dissociation efficiency, $\alpha = 50\%$, is achieved for $Cl_2 = 0.5$ mmol s^{-1} and $P = 15$ torr. This cursory analysis clearly indicates that Cl_2 is inferior to F + HCl/DCl as a Cl atom source. As a result, no model calculations were performed.

Conclusions

The present results demonstrate the utility of the diode laser as a probe of atom flow rates and temperatures. Based on the experimental data and one-dimensional fluid mechanical modeling results, we have established the efficiency of our dc discharge for generation of large F and Cl atom densities. The X + HI titration reactions effectively convert the F and Cl atoms to iodine atoms, which are detected by near IR laser absorption. This method has clear advantages over alternative techniques such as resonance fluorescence or absorption, Cl_2 recombination afterglow, and HF ($\Delta v = 3$) chemiluminescence. Specifically, the laser probe technique gives both atom densities and temperatures and can give two-dimensional spatial resolution when the beam is translated along the vertical and streamwise axes of the reactor. When the path length is increased, extremely low concentrations can be measured.

References

[1]Gross, R. W. F., and Bott, J. F., "Kinetics of Hydrogen-Halide Lasers," *Handbook of Chemical Lasers*, Wiley, New York, 1976, pp. 33–94.

[2]Levine, R. D., and Kinsey, J. L., "Information-Theoretic Approach: Application to Molecular Collisions," *Atom Molecule Collision Theory*, edited by R. B., Bernstein, Plenum, New York, 1979, pp. 693–746.

[3]Herbelin, J. M., Henshaw, T. L., Rafferty, B. D., Anderson, B. T., Tate, R. F., Madden, T. J., Manke, G. C., II, and Hager, G. D., "The Measurement of Gain on the 1.315 μm Transition of Atomic Iodine in a Subsonic Flow of Chemically Generated NCl($a^1\Delta$)," *Chemical Physics Letters*, Vol. 299, Jan. 1999, pp. 583–588.

[4]Ray, A. J., and Coombe, R. D., "An I* Laser Pumped by NCl($a^1\Delta$)," *Journal of Physical Chemistry*, Vol. 99, No. 20, 1995, pp. 7849–7852.

[5]Yang, T. T., Gylys, V. T., Bower, R. D., and Rubin, L. F., "Population Inversion Between I*($^2P_{1/2}$) and I($^2P_{3/2}$) of Atomic Iodine Generated by the Energy Transfer from NCl($a^1\Delta$) to I($^2P_{3/2}$)," *Optics Letters*, Vol. 17, No. 24, 1992, pp. 1803–1805.

[6]Bower, R. D., and Yang, T. T., "I*($^2P_{1/2}$) Produced by the Energy Transfer from NCl($a^1\Delta$) to I($^2P_{3/2}$)," *Journal of the Optical Society of America B—Optical Physics*, Vol. 8, No. 8, 1991, pp. 1583–1587.

[7]Henshaw, T. L., Manke, G. C., II, Madden, T. J., Berman, M. R., and Hager, G. D., "A New Energy Transfer Chemical Laser at 1.315 μm," *Chemical Physics Letters*, Vol. 325, July 2000, pp. 537–544.

[8]McDermott, W. E., Pchelkin, N. R., Benard, D. J., and Bousek, R. R., "An Electronic Transition Chemical Laser," *Applied Physics Letters*, Vol. 32, No. 8, 1978, pp. 469, 470.

[9]Baulch, D. L., Duxbury, J., Grant, S. J., and Montague, D. C., "Evaluated Kinetic Data for High Temperature Reactions Vol. 4, Homogeneous Gas Phase Reactions of Halogen- and Cyanide-Containing Species," *Journal of Physical Chemistry Reference Data*, Vol. 10, Supplement 1, 1981.

[10]Lilenfeld, H. V., Bradburn, G. R., and Hovis, F. E., "Oxygen Iodine Laser Kinetics," Air Force Weapons Lab., AFWL-TR-84-151, Kirtland AFB, NM, 1985.

[11]Hewett, K. B., Manke, G. C., II, Setser, D. W., and Brewood, G., "Quenching Rate Constants of NCl($a^1\Delta$) at Room Temperature," *Journal of Physical Chemistry A*, Vol. 104, No. 3, 2000, pp. 539–551.

[12]Rafferty, B. D., Anderson, B. T., Henshaw, T. L., Herbelin, J. M., and Hager, G. D., "Titration of Fluorine Atoms by Laser Absorption of Iodine Atoms," *Proceedings of the International Conference on Lasers 97*, STS Press, McLean, VA, 1998, pp. 23–28.

[13]Jones, W. E., Skolnik, E. G., "Reactions of Fluorine Atoms," *Chemical Reviews*, Vol. 76, No. 5, 1976, pp. 563–592.

[14]Clyne, M. A. A., Cruse, H. W., and Watson, R. T., "Measurement of Ground State $^2P_{1/2}$ Bromine and Chlorine Atom Concentrations in Discharge-Flow Systems," *Journal of the Chemistry Society, Faraday Transactions 2*, Vol. 68, 1972, pp. 153–168.

[15]Clyne, M. A. A., and Nip, W. S., "Generation and Measurement of Atom and Radical Concentrations in Flow Systems," *Reactive Intermediates in the Gas Phase*, edited by D. W. Setser, Academic Press, New York, 1979, pp. 1–59.

[16]Herzberg, G., and Spinks, J. W. T., *Atomic Spectra and Atomic Structure*, Dover, New York, 1944.

[17]Davies, P. B., and Russell, D. K., "Detection of the Chlorine Atom Using a Tunable Diode Laser," *Chemical Physics Letters*, Vol. 67, No. 2–3, 1979, pp. 440, 441.

[18]Laguna, G. A., and Beattie, W. H., "Direct Absorption Measurement of the Spin-Orbit Splitting of the Ground State of Atomic Fluorine," *Chemical Physics Letters*, Vol. 88, No. 4, 1982, pp. 439, 440.

[19]Du, K. Y., and Setser, D. W., "Quenching Rate Constants of NF($a^1\Delta$) at Room Temperature," *Journal of Physical Chemistry*, Vol. 94, No. 6, 1989, pp. 2425–2435.

[20]Wickramaaratchi, M. A., and Setser, D. W., "Infrared Chemiluminescence of Cl + HI, HBr, DBr, PH_3, PD_3, and GeH_4: Vibrational Energy Disposal and Rate Constants," *Journal of Physical Chemistry*, Vol. 87, No. 1, 1983, pp. 64–72.

[21]Howard, C. J., "Kinetic Measurements Using Flow Tubes," *Journal of Physical Chemistry*, Vol. 83, No. 1, 1979, pp. 3–9.

[22]Shapiro, A. H., *The Dynamics and Thermodynamics of Compressible Fluid Flow*, Vol. 1, Wiley, New York, 1953, pp. 219–262.

[23]Kuo, K. K., *Principles of Combustion*, Wiley, New York, 1986, p. 102.

[24]Lilenfeld, H. V., and Bradburn, G. R., "Rate Constant for the Reaction $I + F_2 \rightarrow IF + F$," *Journal of Physical Chemistry*, Vol. 91, No. 7, 1987, pp. 1881–1883.

[25]Kota, G. P., Coburn, J. W., and Graves, D. B., "Heterogeneous Recombination of Atomic Bromine and Fluorine," *Journal of Vacuum Science and Technology A—Vacuum Surfaces and Films*, Vol. 17, No. 1, 1999, pp. 282–290.

[26]Perram, G. P., and Hager, G. D., "The Standard Chemical Oxygen–Iodine Laser Kinetics Package," Air Force Weapons Lab., AFWL-TR-88-50, Kirtland AFB, NM, Oct. 1988.

[27]Fisk, G. A., and Hays, G. N., "Kinetic Rates in the Oxygen–Iodine System," *Journal of Chemical Physics*, Vol. 77, No. 10, 1982, pp. 4965–4971.

[28]Coombe, R. D., and Pritt, A. T., Jr., "Electronic to Vibrational Energy Transfer $I^*5\,^2P_{1/2}$ to HF," *Journal of Chemical Physics*, Vol. 66, No. 11, 1977, pp. 5214–5219.

[29]Berman, M. R., and Whitefield, P. D., "Collisional Deactivation of $I(5\,^2P_{1/2})$ by F_2," *Journal of Chemical Physics*, Vol. 84, No. 8, 1986, pp. 4281–4287.

[30]Grimley, A. J., and Houston, P. L., "Electronic to Vibrational Energy Transfer from $I^*5\,^2P_{1/2}$ I. HCl, HBr, and NO," *Journal of Chemical Physics*, Vol. 68, No. 8, 1978, pp. 3368–3376.

[31]Chowdhury, M. A., Pritt, A. T., Patel, D., and Benard, D. J., "Quenching of $I^*(5\,^2P_{1/2})$ by Halogen Fluorides," *Journal of Chemical Physics*, Vol. 84, No. 12, 1986, pp. 6687–6693.

[32]Chang, H. W., and Burns, G. J., "Recombination of Iodine Atoms by Flash Photolysis over a Wide Temperature Range. VII. Recombination Between 206 and 300 K," *Journal of Chemical Physics*, Vol. 64, No. 1, 1976, pp. 349–353.

[33]Cohen, N., and Bott, J. F., "A Review of Rate Coefficients in the H_2-F_2 Chemical Laser System," Space and Missile Systems Organization, TR-76-82, Los Angeles, 1976.

[34]Kota, G. P., Coburn, J. W., and Graves, D. B., "The Recombination of Chlorine Atoms at Surfaces," *Journal of Vacuum Science and Technology A—Vacuum Surfaces and Films*, Vol. 16, No. 1, 1998, pp. 270–277.

[35]Press, W. H., Flannery, B. P., Teukolsky, S. A., and Vetterling, W. T., *Numerical Recipes: The Art of Scientific Computing (Fortran Version)*, Cambridge Univ. Press, Cambridge, England, U.K., 1989, pp. 570, 571.

R. P. Lucht
Associate Editor